

Trajectories of light beams in a Kerr metric: the influence of the rotation of an observer on the shadow of a black hole

I.A. Bizyaev

*Ural Mathematical Center, Udmurt State University, ul. Universitetskaya 1, 426034 Izhevsk, Russia**

This paper investigates the trajectories of light beams in a Kerr metric, which describes the gravitational field in the neighborhood of a rotating black hole. After reduction by cyclic coordinates, this problem reduces to analysis of a Hamiltonian system with two degrees of freedom. A bifurcation diagram is constructed and a classification is made of the types of trajectories of the system according to the values of first integrals. Relations describing the boundary of the shadow of the black hole are obtained for a stationary observer who rotates with an arbitrary angular velocity about the axis of rotation of the black hole.

INTRODUCTION

An analysis of the trajectory of light beams for a Kerr metric has been carried out by Bardeen [1]. He analyzed how the rotation of a black hole influences the form of its shadow against a brightly glowing background which is far away from the event horizon. Interestingly, it turned out that this shadow is asymmetric with respect to the axis of rotation of the black hole and, as pointed out in [12], resembles the forms of letter D.

A detailed discussion of subsequent studies of the trajectories of light beams in a Kerr metric is presented in [6, 16, 17]. In those studies, the shadow of the black hole is usually considered in a locally nonrotating reference system which is sufficiently far away from the event horizon. An exception is Ref. [9], in which an equation was obtained for the boundary of the shadow of the black hole for a Carter observer for whom the radial coordinate is larger than the maximal radial coordinate of the spherical photon orbit.

This paper continues the investigation of the geodesics of a Kerr metric using methods of qualitative analysis. Previously, a bifurcation diagram was constructed in [2] for timelike geodesics. It was shown that there exist seven different regions of values of first integrals which differ in the topological type of integral submanifold. This paper is concerned with the isotropic geodesics of a Kerr metric. In Section II, a bifurcation diagram is constructed and a classification is made of the types of trajectories of light beams according to the values of first integrals. Previously, such a diagram was constructed in [10]. In Section III, relations are obtained for the boundary of the shadow of a black hole for a stationary observer who rotates with an arbitrary angular velocity about the axis of rotation of the black hole. In addition, a backward tracing of light beams is constructed and it is shown how the image for the observer changes as the event horizon is approached.

The growing interest in research on the shadow of a black hole is fueled by images obtained recently of supermassive objects M87* in the center of galaxy M87 and SgA* in the center of our galaxy. Examination of these images reveals a bright accretion substance reaching the event horizon and radiating in its vicinity. In this paper, we will not consider the image due to an accretion disk. Such an image is discussed in detail, for example, in [6, 12, 14].

* bizyaevtheory@gmail.com

I. EQUATIONS OF MOTION OF LIGHT BEAMS

In the Boyer–Lindquist coordinates $\mathbf{x} = (t, r, \theta, \varphi)$ the interval (line element) for a Kerr metric g_{ij} is represented as follows [4]:

$$\begin{aligned} ds^2 = g_{ij}dx^i dx^j &= -\frac{\rho^2 \Delta(r)}{A} dt^2 + \frac{A}{\rho^2} \sin^2 \theta (d\varphi - \omega dt)^2 + \rho^2 \left(\frac{dr^2}{\Delta(r)} + d\theta^2 \right), \\ \rho^2 &= r^2 + a^2 \cos^2 \theta, \quad \Delta(r) = r^2 - 2r + a^2, \\ A &= (r^2 + a^2)^2 - a^2 \Delta(r) \sin^2 \theta, \quad \omega = \frac{2ra}{A}, \end{aligned} \quad (1)$$

where the signature $(-, +, +, +)$ is chosen and the coordinates r and t are measured in the following units:

$$\frac{GM}{c^2}, \quad \frac{GM}{c^3},$$

where G is the gravitational constant, c is the velocity of light, and M is the mass of the black hole.

The dimensionless parameter a is expressed in terms of the angular momentum of the black hole J relative to the symmetry axis as follows:

$$a = \frac{Jc}{GM^2}.$$

At large distances, i.e., at $r \gg 1$ the metric (1) becomes a flat Minkowski metric:

$$ds^2 = dt^2 - \rho^2 \left(\frac{dr^2}{r^2 + a^2} + d\theta^2 \right) - (r^2 + a^2) \sin^2 \theta d\varphi^2 = dt^2 - dx^2 - dy^2 - dz^2,$$

where the Cartesian coordinates are given by the following relations:

$$x = \sqrt{r^2 + a^2} \sin \theta \cos \varphi, \quad y = \sqrt{r^2 + a^2} \sin \theta \sin \varphi, \quad z = r \cos \theta. \quad (2)$$

It follows from relations (2) that the level surfaces of the *radial coordinates* $r = \text{const}$ at $t = \text{const}$ are confocal spheroids in the three-dimensional space

$$\frac{x^2 + y^2}{r^2 + a^2} + \frac{z^2}{r^2} = 1.$$

The variables $\theta \in (0, \pi)$ and $\varphi \in [0, 2\pi)$ are *polar* and *azimuth angles*, respectively, and the coordinate t plays the role of the *time* of an external observer at rest.

The surface defining the *event horizon* for the metric (1) is represented as

$$\begin{aligned} \mathcal{S}_h &= \{(t, r, \theta, \varphi) \mid r = r_+\}, \\ r_+ &= 1 + \sqrt{1 - a^2}, \end{aligned} \quad (3)$$

where r_+ is the dominant root of the equation $\Delta(r) = 0$. According to (3), for an event horizon to exist, the value r_+ must be real. This leads to the condition $a \leq 1$. Furthermore, without loss of generality we will assume that $a \geq 0$.

In what follows, we will consider the trajectories of light beams only on the “outer” side of the event horizon \mathcal{S}_h , i.e., on the manifold

$$\mathcal{N}^4 = \{(t, r, \theta, \varphi) \mid t \in (-\infty, +\infty), r \in (r_+, +\infty), \theta \in (0, \pi), \varphi \in [0, 2\pi)\}.$$

We note that in this case the inequality $\rho(r, \theta) > 0$ is satisfied.

The equations of motion for geodesics can be represented in the following Hamiltonian form:

$$\begin{aligned} \frac{dx^i}{d\tau} &= \frac{\partial H}{\partial p_i}, \quad \frac{dp_i}{d\tau} = -\frac{\partial H}{\partial x^i}, \quad i = 1, \dots, 4, \\ H &= \frac{1}{2} g^{ij} p_i p_j, \end{aligned} \quad (4)$$

where $\mathbf{p} = (p_t, p_r, p_\theta, p_\varphi)$ is the four-momentum along the trajectory and g^{ij} is the matrix inverse to the metric defined by relation (1).

The metric g_{ij} does not depend explicitly on time t and the angle φ , and hence they are cyclic coordinates for equations (4). As a consequence, the corresponding momenta remain unchanged:

$$E = -p_t = \text{const}, \quad L = p_\varphi = \text{const},$$

and the Hamiltonian system with two degrees of freedom decouples from the system (4):

$$\frac{dp_r}{d\tau} = -\frac{\partial H}{\partial r}, \quad \frac{dp_\theta}{d\tau} = -\frac{\partial H}{\partial \theta}, \quad \frac{dr}{d\tau} = \frac{\partial H}{\partial p_r}, \quad \frac{d\theta}{d\tau} = \frac{\partial H}{\partial p_\theta}. \quad (5)$$

The trajectories of light beams lie on the zero level set of the Hamiltonian of this system:

$$H = \frac{1}{2\rho^2} (\Delta(r)p_r^2 + p_\theta^2) + U(r, \theta) = 0, \quad (6)$$

$$U(r, \theta) = \frac{1}{2\Delta(r)\rho^2} \left(4arEL + \frac{\Delta(r)L^2}{\sin^2 \theta} - a^2 L^2 \right) - \left(\frac{1}{2} + \frac{r(r^2 + a^2)}{\Delta(r)\rho^2} \right) E^2,$$

where the function $U(r, \theta)$ is the effective potential.

According to the well-known solution to the system (5), the evolution of the remaining variables is defined from the equations

$$\frac{d\varphi}{d\tau} = \frac{a}{\Delta(r)\rho^2} (E(r^2 + a^2) - aL) - \frac{aE}{\rho^2} + \frac{L}{\rho^2 \sin^2 \theta}, \quad (7)$$

$$\frac{dt}{d\tau} = \frac{r^2 + a^2}{\Delta(r)\rho^2} (E(r^2 + a^2) - aL) + \frac{a}{\rho^2} (L - aE \sin^2 \theta).$$

In addition to the Hamiltonian H , the reduced system (5) has an additional Carter integral [5]

$$F = p_\theta^2 + \left(aE \sin \theta - \frac{L}{\sin \theta} \right)^2 - 2a^2 H \cos^2 \theta. \quad (8)$$

For a more detailed discussion of the physical meaning of the Carter integral, see [13]. Thus, we obtain the following well-known result: the Hamiltonian system (5) is integrable in the Liouville–Arnold sense.

II. BIFURCATION DIAGRAM AND CLASSIFICATION OF TRAJECTORIES

Both integrals of the system (5) are quadratic in the momenta, and hence this system can be integrated by the method of separation of variables (for details, see [8]). In this case, r and θ are separating variables. Therefore, in order to reduce the problem to quadratures, we fix the common level set of the Carter integral:

$$F = Q + (L - aE)^2, \quad (9)$$

where Q is some constant.

To analyze the trajectories of light beams, it is convenient to introduce the quantities

$$\lambda = \frac{L}{E}, \quad \eta = \frac{Q}{E}, \quad (10)$$

then we express the momenta p_r and p_θ from (6) and (8) using (9) and substitute them into the last two equations of motion of the system (5). As a result, we obtain equations for r and θ in the following form:

$$\left(\frac{dr}{d\tau} \right)^2 = \frac{E^2}{\rho^4} R(r), \quad \left(\frac{d\theta}{d\tau} \right)^2 = \frac{E^2}{\rho^4} \Theta(\theta), \quad (11)$$

$$R(r) = (r^2 + a^2 - a\lambda)^2 - (\eta + (\lambda - a)^2) \Delta(r),$$

$$\Theta(\theta) = \eta + \cos^2 \theta \left(a^2 - \frac{\lambda^2}{\sin^2 \theta} \right).$$

As can be seen, in order to integrate these equations in explicit form, we need to rescale time as

$$d\tau = \frac{\rho^2(r, \theta)}{E} d\sigma. \quad (12)$$

Using the new time variable and relations (10), we rewrite the system (7) as

$$\frac{d\varphi}{d\sigma} = \frac{a}{\Delta(r)} (r^2 + a^2 - a\lambda) - a + \frac{\lambda}{\sin^2 \theta}, \quad (13)$$

$$\frac{dt}{d\sigma} = \frac{r^2 + a^2}{\Delta(r)} (r^2 + a^2 - a\lambda) + a(\lambda - a \sin^2 \theta). \quad (14)$$

We first analyze the trajectories of equations (11). For them it holds that

– the *region of possible motion* on the plane $\mathbb{R}^2 = \{(r, \theta) \mid r > r_+, \theta \in (0, \pi)\}$ is defined by the relations

$$R(r) \geq 0, \quad \Theta(\theta) \geq 0; \quad (15)$$

– the simple zeros r_u and θ_u of the functions

$$R(r_u) = 0, \quad \Theta(\theta_u) = 0$$

define the *turning points* of the variables r and θ , respectively.

– those zeros r_c and θ_c which are simultaneously the critical points

$$R(r_c) = 0, \quad \left. \frac{dR}{dr} \right|_{r=r_c} = 0, \quad (16)$$

$$\Theta(\theta_c) = 0, \quad \left. \frac{d\Theta}{d\theta} \right|_{\theta=\theta_c} = 0, \quad (17)$$

define the invariant manifolds $r = r_c = \text{const}$ and $\theta = \theta_c = \text{const}$.

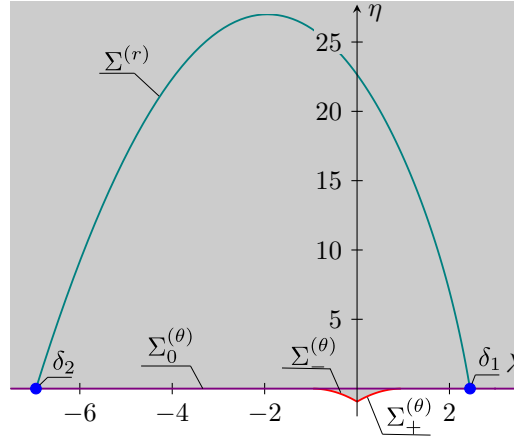


Figure 1: Bifurcation diagram for the fixed $a = 0.97$. Gray denotes the values of the integrals for which inequalities (15) are satisfied.

Thus, investigation of the trajectories of light beams reduces to analysis of the behavior of the functions $R(r)$ and $\Theta(\theta)$ depending on the values of the first integrals λ and η .

Solving relations (16) for λ , η and choosing those values for which inequalities (15) hold, we obtain a parametrically given curve on the plane of first integrals

$$\Sigma^{(r)} = \left\{ (\lambda, \eta) \mid \lambda = \frac{(1+r_c)a^2 + r_c^2(r_c-3)}{a(1-r_c)}, \eta = r_c^3 \frac{4a^2 - r_c(r_c-3)^2}{a^2(r_c-1)^2}, r_c \in [r_1, r_2] \right\},$$

$$r_1 = 2 + 2 \cos\left(\frac{2}{3} \arccos(-a)\right), \quad r_2 = 2 + 2 \cos\left(\frac{2}{3} \arccos(a)\right)$$

Solving relations (17) for the values of the first integrals, we obtain the straight line $\Sigma_0^{(\theta)} = \{(\lambda, \eta) \mid \eta = 0\}$ for which $\theta_c = \frac{\pi}{2}$, and two curves

$$\Sigma_{\pm}^{(\theta)} = \{(\lambda, \eta) \mid \lambda = \pm a \sin^2 \theta_c, \eta = -a^2 \cos^4 \theta_c, \theta_c \in (0, \pi)\},$$

where the upper sign corresponds to $\Sigma_+^{(\theta)}$, and the lower sign, to $\Sigma_-^{(\theta)}$.

The curve $\Sigma^{(r)}$ intersects with the straight line $\Sigma_0^{(\theta)}$ at two points, which we denote by δ_1 and δ_2 . They correspond to the fixed points of the reduced system (5) lying in the equatorial plane $\theta = \frac{\pi}{2}$ and to the values of the radial coordinate, r_1 and r_2 , for δ_1 and δ_2 , respectively.

REMARK 1. Equations (16) have another solution, namely,

$$\eta = -\frac{r_c^4}{a^4}, \quad \lambda = \frac{a^2 + r_c^2}{a},$$

but it must be eliminated because in this case

$$\Theta(\theta) = -\frac{(r_c^2 + a^2 \cos^2 \theta)^2}{a^2 \sin^2 \theta} < 0.$$

Typical curves found on the plane of first integrals are shown in Fig. 1. As is well known from the analysis of the function of a real variable, changes in the region of possible motion (15) and in the number of the turning points r_u or θ_u occur for the values of the first integrals lying on these bifurcation curves [3].

REMARK 2. The bifurcation curves thus found describe local bifurcations. No nonlocal bifurcations due to changes in the behavior of the function $R(r)$ arise on the boundaries of the interval $(r_+, +\infty)$. Nonlocal bifurcations arise for the motion of a material point (i.e., $H = 1/2$) and are examined in detail in [2].

REMARK 3. The bifurcation diagram shows the point $(0, -a^2)$ at which the curves $\Sigma_-^{(\theta)}$ and $\Sigma_+^{(\theta)}$ merge. This point corresponds to the trajectory that lies entirely on the symmetry axis.

Figure 2 shows examples of the functions $\Theta(\theta)$ and $R(r)$ with different numbers of turning points. Note that, if $\eta < 0$, then the trajectories do not cross the equatorial plane. Moreover, the inequality $\frac{dt}{d\sigma} > 0$ always holds in the region of possible motion, and so we will not analyze the dependence $t(\sigma)$ in detail.

Critical solutions for which $r(\sigma) = r_c$ are called spherical orbits. They are examined in detail in [18]. For the points δ_1 and δ_2 they reduce to flat trajectories which are circles. Furthermore, for δ_2 the direction of rotation does not coincide with the direction of rotation of the black hole since in this case $\frac{d\varphi}{d\sigma} < 0$, whereas for δ_1 the direction of rotation does coincide with the direction of rotation of the black hole since $\frac{d\varphi}{d\sigma} > 0$.

Let us consider in more detail the behavior of the function $r(\sigma)$ depending on the values of the first integrals. According to the bifurcation diagram, two cases should be distinguished.

- (i) If the point (λ, η) lies below the curve $\Sigma^{(r)}$, then the turning point r_u is absent and all trajectories, as they continue in τ in one direction, go to infinity ($r \rightarrow +\infty$), and as they continue in τ in the opposite direction, they approach the horizon. In this paper, we call such trajectories the ‘‘horizon/infinity’’.
- (ii) If the point (λ, η) lies above the curve $\Sigma^{(r)}$, then there are two turning points r_u . One turning point corresponds to a trajectory of the type ‘‘horizon/horizon’’, and the other, to a trajectory of the type ‘‘infinity/infinity’’.

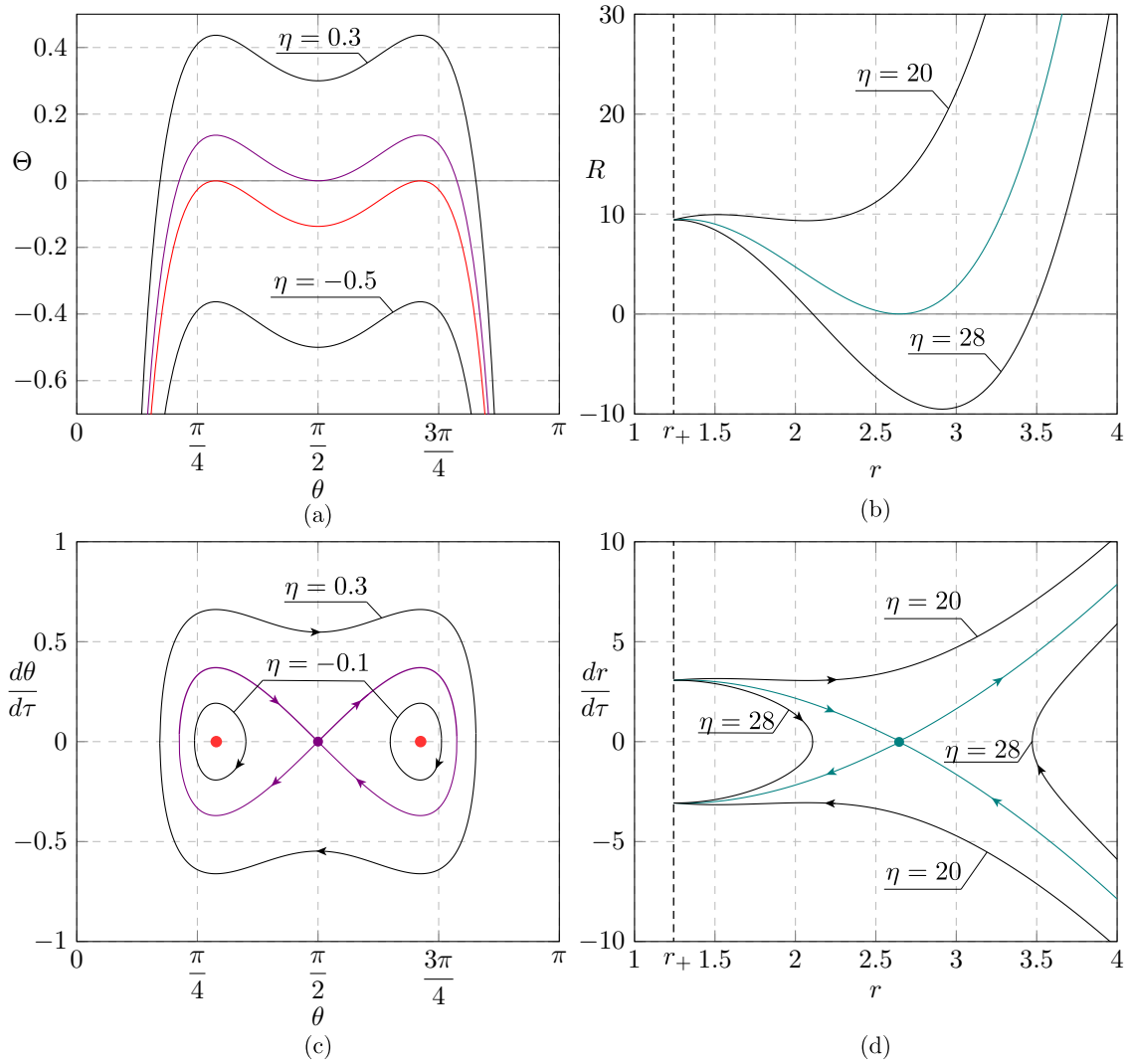


Figure 2: For fixed $\lambda = -0.6$ and $a = 0.97$ (a) the function $\Theta(\theta)$, (b) the function $R(r)$, and (c)-(d) the phase portraits, versus η . The colored curves in these figures are plotted for the values of the first integrals lying on the bifurcation curves shown in the same colors in Fig. 1.

In each of these regions the solution is given in terms of elliptic functions (for details, see, e.g., [10, 11]). For the values of the integrals lying on the curve $\Sigma^{(r)}$ in the phase portrait of the system (see Fig. 2d) there are a saddle fixed point and asymptotic trajectories adjacent to it (*separatrices*).

For the separatrices the solution $r(\sigma)$ can be expressed in elementary functions. In order to obtain it, we substitute into the function $R(r)$ the values of the integrals λ and η on the curve $\Sigma^{(r)}$ and represent this function as

$$R(r) = \pm(r - r_c)\sqrt{r^2 + 2r_cr - 3r_c^2 + Z^2},$$

$$Z = \frac{2\sqrt{r_c}}{1 - r_c}(3r_c - (a^2 + 3r_c^2) + r_c^3)^{1/2}. \quad (18)$$

Integrating the first of equations (11) using the new time variable (12), we find an expression for the separatrix which, for the initial value of the radial coordinate $r(0) > r_c$, approaches asymptotically the solution $r = r_c$:

$$r(\sigma) = r_c + Z^2(r(0) - r_c)\left((Z^2 + 2r_c(r(0) - r_c)) \cosh(Z\sigma) + Z\sqrt{Z^2 + (r(0) + r_c^2) - 4r_c^2} \sinh(Z\sigma) - 2r_c(r(0) - r_c)\right)^{-1}. \quad (19)$$

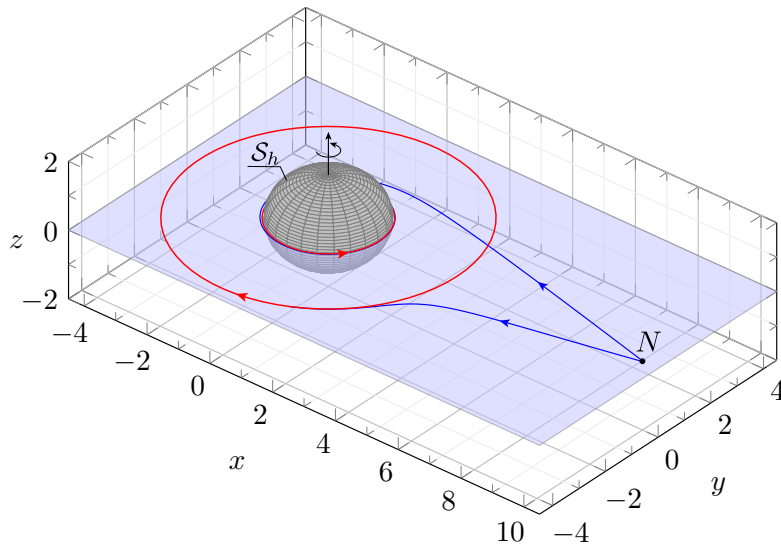


Figure 3: Typical circular trajectories (red) and separatrices (light blue) for the fixed parameter $a = 0.97$ and the initial conditions $r(0) = 10$ and $\varphi(0) = 0$, which correspond to point N .

Figure 3 shows separatrices lying in the equatorial plane $\theta = \frac{\pi}{2}$. For them, the dependence $\varphi(\sigma)$ was obtained after integration of equation (13) taking (19) into account. The flat trajectories with the initial conditions from point N which lie between the separatrices plunge into the event horizon, and the other trajectories go to infinity. Note that an asymmetry arises in these plunging trajectories with respect to the axis of rotation of the black hole, which is caused by the positions of the unstable circular orbits. As the parameter a increases, this asymmetry becomes more pronounced because the distance between the unstable circular orbits increases.

III. STATIONARY REFERENCE SYSTEMS AND THE SHADOW OF THE BLACK HOLE

Consider reference systems which outside the horizon \mathcal{S}_h rotate about the axis of rotation of the black hole with constant angular velocity Ω . For them, the space-time remains stationary, and hence we will call them *stationary reference systems* [19]. Suppose that at the origin of such a reference system there is an observer for whom the Boyer–Lindquist coordinates are given by the following relations:

$$r = r_0 = \text{const}, \quad \theta = \theta_0 = \text{const}, \quad \varphi = \Omega t + \varphi_0.$$

For such a stationary observer the four-velocity has the following form:

$$\mathbf{u} = u_0 \left(\frac{\partial}{\partial t} + \omega_0 \frac{\partial}{\partial \varphi} \right), \quad u_0 = \frac{dt}{d\tau} = \rho_0 \left(\Delta(r_0) - a^2 \sin^2 \theta_0 + \Omega(4ar_0 - A_0 \Omega) \sin^2 \theta_0 \right)^{-1/2},$$

where τ is the proper time and the following notation is used:

$$\rho_0^2 = r_0^2 + a^2 \cos^2 \theta_0, \quad A_0 = (r_0^2 + a^2)^2 - a^2 \Delta(r_0) \sin^2 \theta_0, \quad \omega_0 = \frac{2r_0 a}{A_0}.$$

In order that the observer's trajectory remain timelike, the radicand for u_0 must take positive values. From this we obtain the following range of admissible angular velocities:

$$\Omega \in (\Omega_-, \Omega_+), \quad \Omega_{\pm} = \frac{1}{r_0^2 + a^2 \pm a \sqrt{\Delta(r_0)} \sin \theta_0} \left(a \pm \frac{\sqrt{\Delta(r_0)}}{\sin \theta_0} \right),$$

where the lower sign corresponds to Ω_- and the upper sign, to Ω_+ .

Table I: Examples of observers in the case of a Kerr metric.

name	angular velocity Ω	time component of velocity u_0
zero angular momentum observer or ZAMO	ω_0	$\frac{1}{\sqrt{\Delta(r_0)}} \left(r_0^2 + a^2 + \frac{2r_0 a^2 \sin^2 \theta_0}{\rho_0^2} \right)^{1/2}$
static observers	0	$\frac{\rho_0}{\sqrt{r_0^2 - 2r_0 + a^2 \cos^2 \theta_0}}$
Carter observers	$\frac{a}{r_0^2 + a^2}$	$\frac{r_0^2 + a^2}{\rho_0 \sqrt{\Delta(r_0)}}$

Examples of observers which are usually given for a Kerr metric are summarized in Table I (for details, see, e.g., [19]). Recall that a static observer can be defined only outside the ergosphere.

The basis vectors of the orthonormal tetrad which are related to the stationary observer have the following form (see Fig. 4a):

$$\begin{aligned} \mathbf{e}_{(t)} = \mathbf{u}, \quad \mathbf{e}_{(r)} = -\frac{\sqrt{\Delta(r_0)}}{\rho_0} \frac{\partial}{\partial r}, \quad \mathbf{e}_{(\theta)} = -\frac{1}{\rho_0} \frac{\partial}{\partial \theta}, \\ \mathbf{e}_{(\varphi)} = \frac{u_0}{\sin \theta_0 \sqrt{\Delta(r_0)}} \left[\frac{A_0 \sin^2 \theta_0}{\rho_0^2} (\Omega - \omega_0) \frac{\partial}{\partial t} + \left(1 - 2r_0 \frac{1 - a\Omega \sin^2 \theta_0}{\rho_0^2} \right) \frac{\partial}{\partial \varphi} \right]. \end{aligned}$$

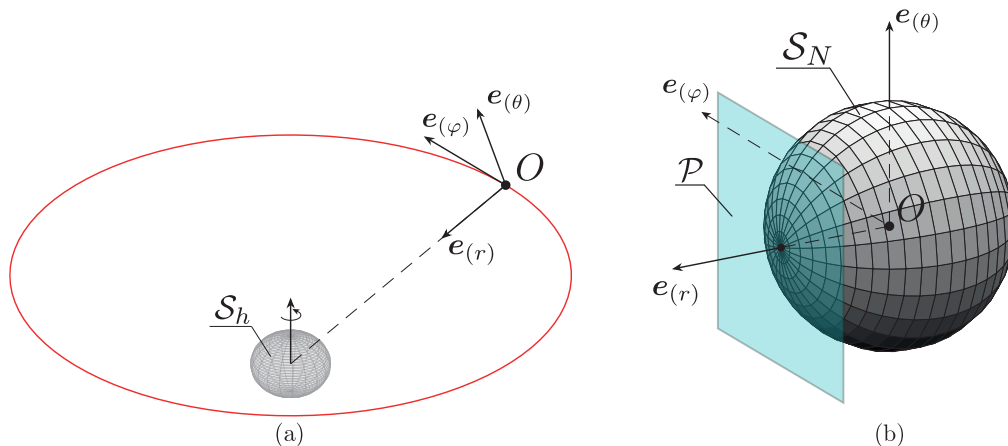


Figure 4: (a) Schematic diagram of the horizon \mathcal{S}_h and (b) schematic diagram of the sphere \mathcal{S}_N and the plane \mathcal{P} relative to the spatial components of the vectors $\mathbf{e}_{(r)}$, $\mathbf{e}_{(\theta)}$ and $\mathbf{e}_{(\varphi)}$.

We describe what a stationary observer must see in the neighborhood of the black hole. Assume that a point source of light beams is at the origin and that these beams evolve backward in time τ . The tangent vector to such an arbitrary light beam is given by the relation

$$\mathbf{w} = W(-\mathbf{e}_{(t)} + N_1 \mathbf{e}_{(\theta)} + N_2 \mathbf{e}_{(\varphi)} + N_3 \mathbf{e}_{(r)}), \quad (20)$$

where the components of the radius vector $\mathbf{N} = (N_1, N_2, N_3)$ lie on the sphere

$$\mathcal{S}_N = \{N_1 = \sin \alpha \cos \beta, N_2 = \sin \alpha \sin \beta, N_3 = \cos \alpha \mid \alpha \in (0, \pi), \beta \in [0, 2\pi)\}.$$

The trajectories with the initial conditions (20) which evolve onto the event horizon will form the shadow of the black hole [1, 16] against the background of light beams from remote sources. In order to describe the boundary of this shadow, we fix the coordinates r_0 and θ_0 of the observer and his angular velocity Ω . Next, we define three

functions which depend on r_c and have the following form:

$$B_\alpha(r_c) = \arccos \left[\frac{(r_0 - r_c) \sqrt{r_0^2 + 2r_c r_0 - 3r_c^2 + Z^2}}{\rho_0 u_0 (1 - \lambda(r_c) \Omega) \sqrt{\Delta(r_0)}} \right], \quad \Theta_*(r_c) = \eta(r_c) + \cos^2 \theta_0 \left(a^2 - \frac{\lambda^2(r_c)}{\sin^2 \theta_0} \right),$$

$$B_\beta(r_c) = \arctan \left[\frac{u_0 (\rho_0^2 (\lambda(r_c) - \Omega (r_0^2 + a^2) \sin^2 \theta_0) + 2r_0 (1 - a \Omega \sin^2 \theta_0) (a \sin^2 \theta_0 - \lambda(r_c)))}{\rho_0 \sin \theta_0 \sqrt{\Delta(r_0)} \sqrt{\Theta_*(r_c)}} \right],$$

where Z is given by (18), and the functions $\lambda(r_c)$ and $\eta(r_c)$ are defined by the values of the integrals for the curve $\Sigma^{(r)}$.

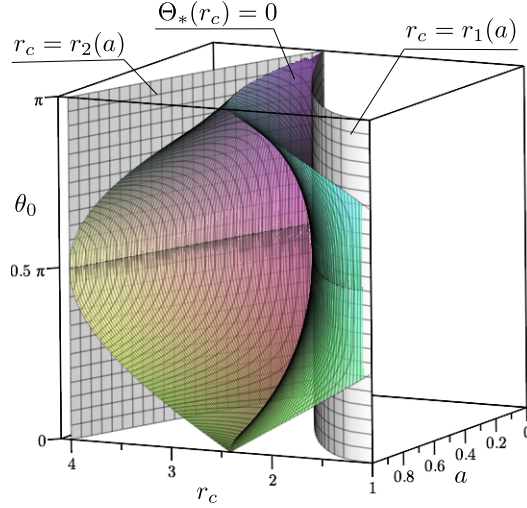


Figure 5: The position of the surface $\Theta_*(r_c) = 0$ relative to the surfaces $r_c = r_1(a)$ and $r_c = r_2(a)$.

The function $\Theta_*(r_c)$ always has two zeros, r_1^* and r_2^* , which satisfy the inequalities (see Fig. 5)

$$r_2 \geq r_2^* > r_1^* \geq r_1.$$

In this case, the following statement holds.

Proposition 1. *The curve describing the boundary of the shadow of the black hole on the sphere \mathcal{S}_N is given as follows:*

1) if $r_0 > r_2^*$, then

$$\mathcal{C} = \{ \alpha = B_\alpha(r_c), \beta = \pi + B_\beta(r_c) \} \cup \{ \alpha = B_\alpha(r_c), \beta = 2\pi - B_\beta(r_c) \}, \quad (21)$$

where $r_c \in [r_1^*, r_2^*]$;

2) if $r_1^* > r_0$, then

$$\mathcal{C} = \{ \alpha = \pi - B_\alpha(r_c), \beta = \pi + B_\beta(r_c) \} \cup \{ \alpha = \pi - B_\alpha(r_c), \beta = 2\pi - B_\beta(r_c) \}, \quad (22)$$

where $r_c \in [r_1^*, r_2^*]$;

3) if $r_2^* \geq r_0 \geq r_1^*$, then the curve \mathcal{C} is given by relations (21) and (22), in which $r_c \in [r_0, r_2^*]$ and $r_c \in [r_1^*, r_0]$, respectively.

Proof. We first express the angles α and β in terms of $\frac{d\theta}{d\tau}$, $\frac{dr}{d\tau}$, L and E . To do so, we represent the tangent vector (20) to the light beam as

$$\mathbf{w} = \frac{dr}{d\tau} \frac{\partial}{\partial r} + \frac{d\theta}{d\tau} \frac{\partial}{\partial \theta} + \frac{d\varphi}{d\tau} \frac{\partial}{\partial \varphi} + \frac{dt}{d\tau} \frac{\partial}{\partial t}. \quad (23)$$

Setting relations (20) and (23) equal to each other, we find

$$\begin{aligned} \frac{dr}{d\tau} &= -\frac{W\sqrt{\Delta(r_0)}}{\rho_0} \cos \alpha, & \frac{dt}{d\tau} &= -Wu_0 \left(1 - \frac{\Omega A_0 - 2ar_0}{\rho_0^2 \sqrt{\Delta(r_0)}} \sin \alpha \sin \beta \sin \theta_0 \right), \\ \frac{d\theta}{d\tau} &= -\frac{W}{\rho_0} \sin \alpha \cos \beta, & \frac{d\varphi}{d\tau} &= -Wu_0 \left(\Omega + \frac{a(a - 2r_0\Omega) \sin^2 \theta_0 - \Delta(r_0)}{\rho_0^2 \sqrt{\Delta(r_0)} \sin \theta_0} \sin \alpha \sin \beta \right). \end{aligned} \quad (24)$$

We rewrite the relations for the integrals as

$$E = \frac{2ar_0 \sin^2 \theta_0}{\rho_0^2} \frac{d\varphi}{d\tau} + \left(1 - \frac{2r_0}{\rho_0^2} \right) \frac{dt}{d\tau}, \quad L = \frac{A_0 \sin^2 \theta_0}{\rho_0^2} \frac{d\varphi}{d\tau} - \frac{2ar_0 \sin^2 \theta_0}{\rho_0^2} \frac{dt}{d\tau}.$$

Let us multiply the second equation by Ω . Subtracting the first equation from it, we obtain an equation that does not depend explicitly on the angles α and β . From this equation we find

$$W = u_0(\Omega L - E).$$

With (10) taken into account, relations (24) yield

$$\cos \alpha = \frac{\rho_0}{u_0 E (1 - \Omega \lambda) \sqrt{\Delta(r_0)}} \frac{dr}{d\tau}, \quad \sin \alpha \cos \beta = \frac{\rho_0}{u_0 (1 - \Omega \lambda)} \frac{d\theta}{d\tau}. \quad (25)$$

With the initial coordinates from the position of the observer, the noncritical trajectories of light beams traveling back in time go to infinity or reach the event horizon. They are separated from each other by two unstable separatrices (in forward time) to a spherical trajectory (for details, see the phase portrait in Fig. 2d). These separatrices correspond to the sought-for values of the angles α and β . As shown previously in Section II, for the separatrices the values of the integrals lie on the bifurcation curve $\Sigma^{(r)}$, and hence λ and η are given by the following relations:

$$\lambda(r_c) = \frac{(1 + r_c)a^2 + r_c^2(r_c - 3)}{a(1 - r_c)}, \quad \eta(r_c) = r_c^3 \frac{4a^2 - r_c(r_c - 3)^2}{a^2(r_c - 1)^2}. \quad (26)$$

Recall that the region of possible motion is defined by inequalities (15). In the case (26) it follows from the second inequality that $r_c \in [r_1^*, r_2^*]$. Moreover, if $r_0 > r_2^*$ then

$$\frac{dr}{d\tau} = \frac{E}{\rho_0^2} \sqrt{R(r_0)}, \quad \frac{d\theta}{d\tau} = \pm \frac{E}{\rho_0^2} \sqrt{\Theta(\theta_0)}, \quad (27)$$

in the first relation, \pm is absent because in this case the inequality $\frac{dr}{d\tau} > 0$ always holds for an unstable separatrix. For $r_1^* > r_0$ we have

$$\frac{dr}{d\tau} = -\frac{E}{\rho_0^2} \sqrt{R(r_0)}, \quad \frac{d\theta}{d\tau} = \pm \frac{E}{\rho_0^2} \sqrt{\Theta(\theta_0)}, \quad (28)$$

in this case the opposite inequality always holds for an unstable separatrix: $\frac{dr}{d\tau} < 0$ (see Fig. 2d).

If $r_2^* \geq r_0 \geq r_1^*$, then for the separatrices in (27) we need to choose $r_c \in [r_0, r_2^*]$, and in (28) we need to choose $r_c \in [r_1^*, r_0]$. Finally, we substitute (27) and (28) into (25) and, after some transformations, we obtain the sought-for relations (21) and (22). \square

REMARK 4. We note that the functions $B_\alpha(r_c)$ and $B_\beta(r_c)$ simplify greatly for Carter observers and hence the values of the angles α and β for the boundary of the shadow of the black hole for $r_0 > r_1$ can be reduced to the relations

$$\sin \alpha = \frac{2\sqrt{\Delta(r_c)}\sqrt{\Delta(r_0)}}{\Delta(r_c) + \Delta(r_0) - r_c^{-1}(r_0 - r_c)^2}, \quad \sin \beta = \frac{a^2 \cos^2 \theta_0 (r_c - 1) - r_c(r_c^2 - 3r_c + 2a^2)}{2ar_c \sqrt{\Delta(r_c)}}.$$

Previously, these relations were obtained in [16].

To visualize the curve \mathcal{C} found above, we perform a stereographic projection of the sphere \mathcal{S}_N onto the plane \mathcal{P} . The position of the plane is shown in Fig. 4b. The Cartesian coordinates on this plane are given by the relations

$$X = 2 \tan \frac{\alpha}{2} \sin \beta, \quad Y = 2 \tan \frac{\alpha}{2} \cos \beta.$$

Figure 6a shows the curve \mathcal{C} on the plane \mathcal{P} plotted against the angle θ_0 . As can be seen, the shadow of the black hole is not axisymmetric, and this asymmetry is seen most clearly for the equatorial plane. Figure 6b shows the shadow of the black hole plotted against the angular velocity Ω in the equatorial plane. Also, Fig. 7 shows how the boundary of the shadow of the black hole changes depending on the radial coordinate of a static observer and a zero angular momentum observer.

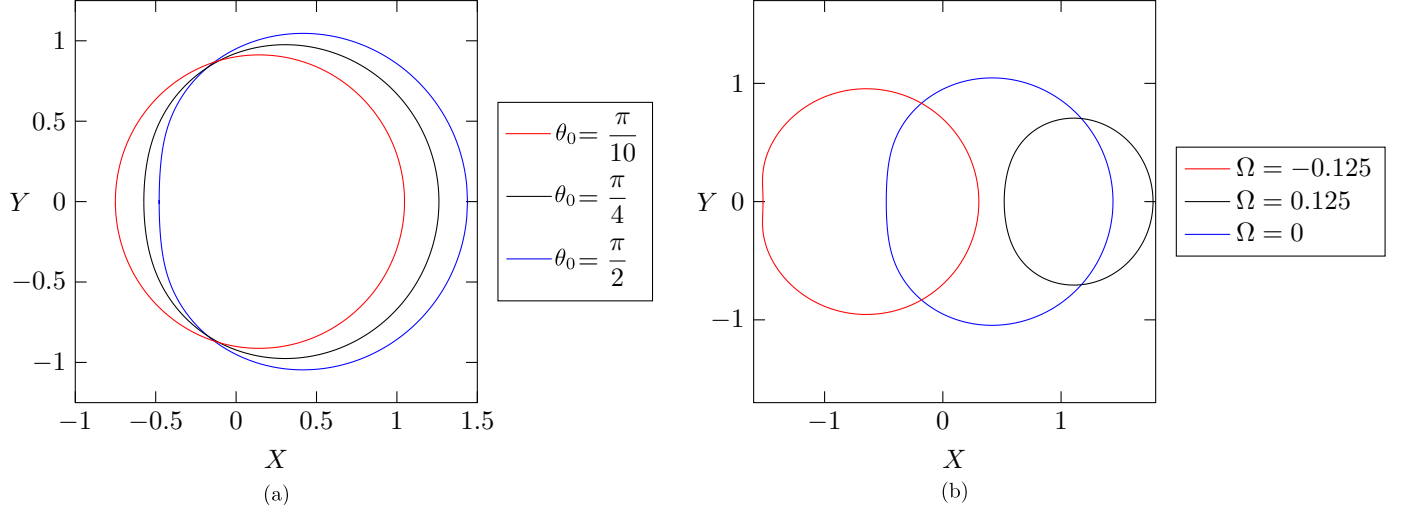


Figure 6: The curve \mathcal{C} for the fixed $a = 0.98$, $r_0 = 5$: (a) different θ_c and the fixed $\Omega = 0$, (b) different Ω and the fixed $\theta_0 = \frac{\pi}{2}$.

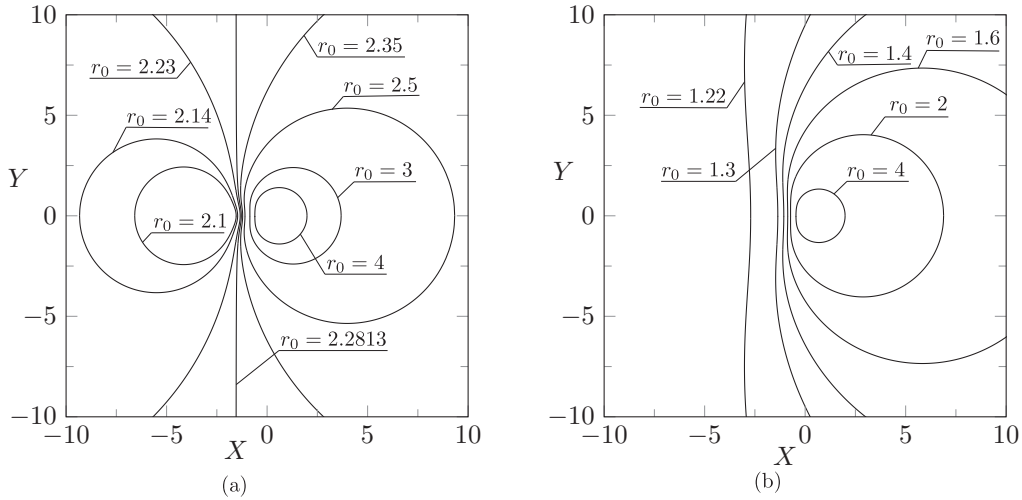


Figure 7: The curve \mathcal{C} for the fixed $a = 0.98$, $\theta_0 = \frac{\pi}{2}$ and different r_0 : (a) for a static observer $\Omega = 0$, (b) for a zero angular momentum observer $\Omega = \omega_0$.

To visualize the image that a stationary observer must see, we perform a backward tracing of light beams [14, 15, 20]. Below we describe briefly its construction.

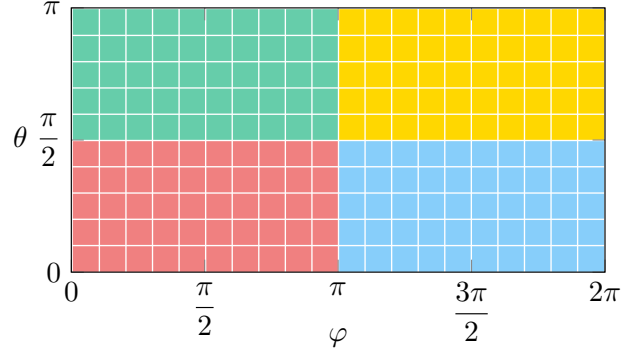


Figure 8: Diagram of the celestial sphere on the plane of angles (φ, θ) .

- Define the celestial sphere as a source of light beams for which the value of the radial coordinate is $r \gg 1$. Since $a \leq 1$, we can neglect in (2) the contribution of the parameter a for the celestial sphere. Single out four regions on the celestial sphere and show them in different colors as depicted in Fig. 8.
- For the fixed initial conditions, from the position of the observer r_0, θ_0 and $\varphi(0) = 0$, but with different values of the angles α and β , we will numerically integrate the system (5) and the first equation in the system (7) in backward time, i.e., after the time reversal $\tau \rightarrow -\tau$.
- On the plane \mathcal{P} , the trajectories of light beams which do not reach the celestial sphere will be shown in black, and the other trajectories will be shown in colors depending on what part of the celestial sphere the trajectory will reach.

The image on the plane \mathcal{P} after the backward tracing of light beams is depicted in Figs. 9 and 10. In these figures one can clearly see a curvature of the trajectories of light beams due to the gravitational field. Moreover, as the radial coordinate decreases, the black region on the plane \mathcal{P} increases. This region corresponds to the shadow of the black hole. The boundary of this region is in agreement with the relations obtained above in Statement 1 (see Fig. 7a).

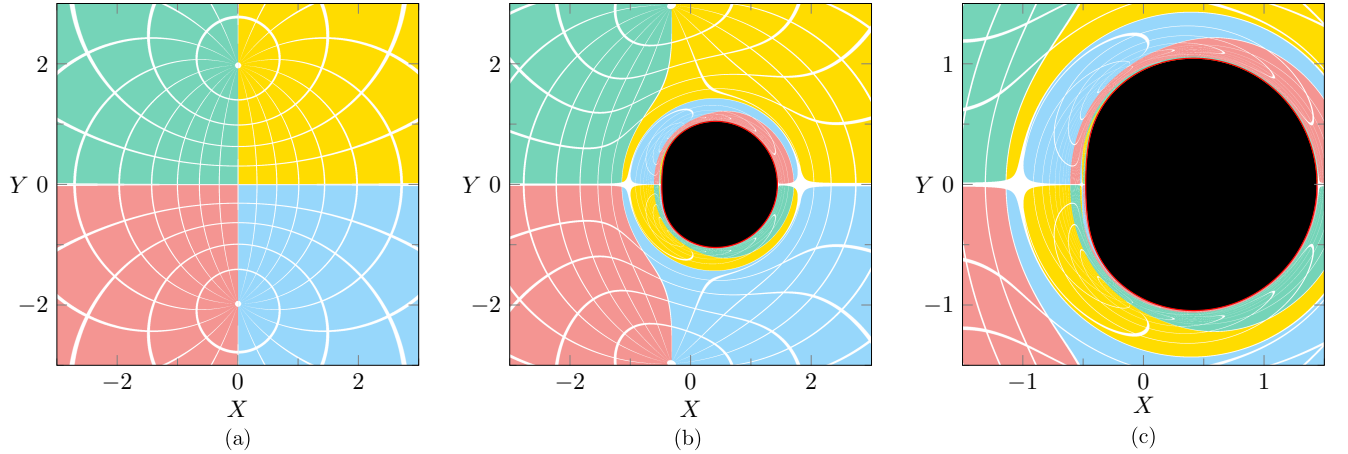


Figure 9: (a) The celestial sphere on the plane \mathcal{P} in the plane space; (b) image on the plane \mathcal{P} in the neighborhood of the black hole after the backward tracing of light beams and (c) enlarged fragment. The observer is in the equatorial plane $\theta_0 = \frac{\pi}{2}$ with $r_0 = 5$ and angular velocity $\Omega = 0$. The celestial sphere is at distance $r = 1000$. Red denotes the shadow's boundary obtained from relations (21).

A classification of trajectories of light beams was carried out within the framework of the state assignment of the Ministry of Science and Higher Education of Russia (FEWS-2024-0007). An analysis of the boundary of the shadow of the black hole and the tracing of light beams was performed at the Ural Mathematical Center (Agreement No. 075-02-2024-1445).

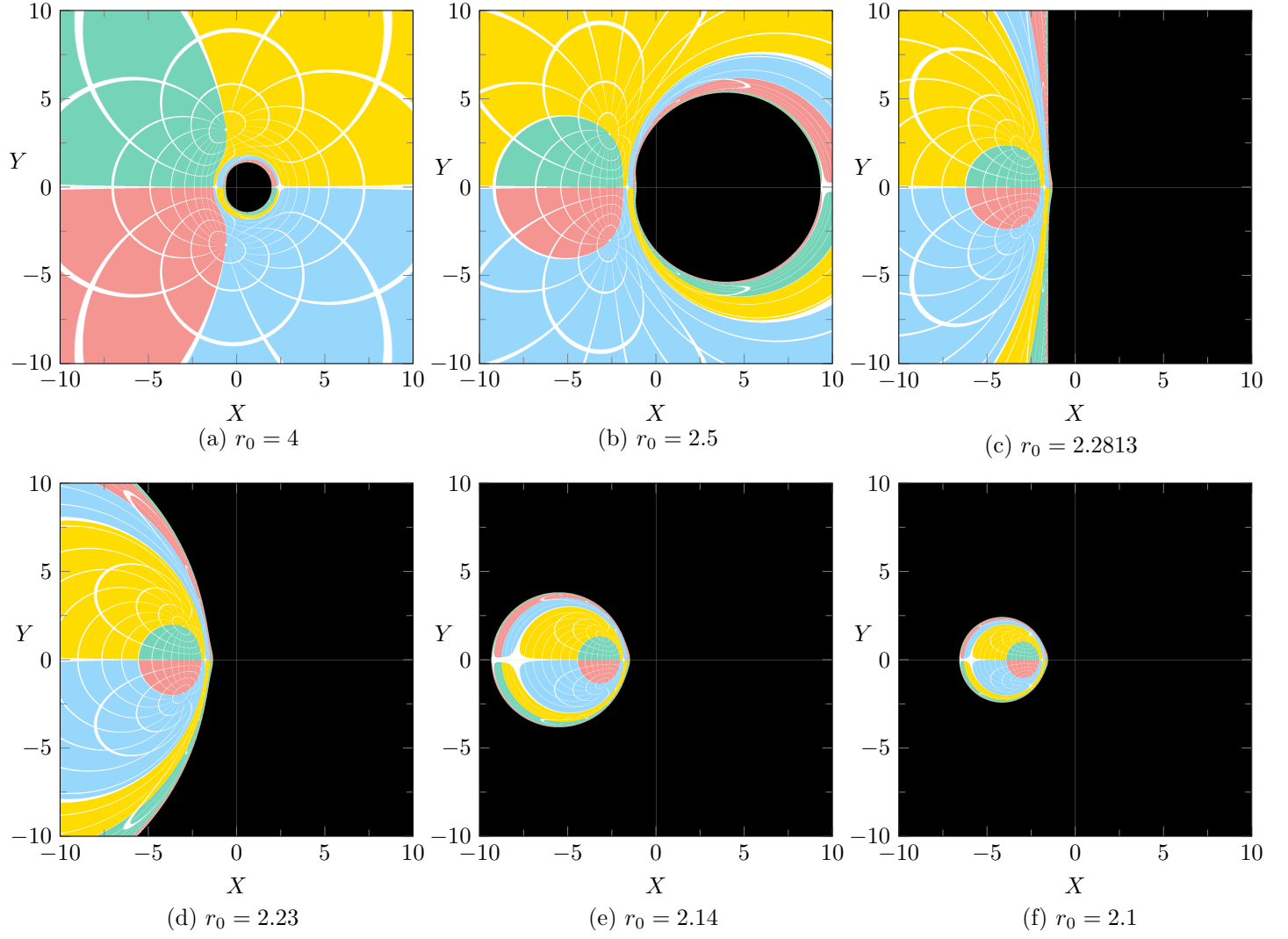


Figure 10: The image on the plane \mathcal{P} in the neighborhood of the black hole after the backward tracing of light beams, plotted against the radial coordinate r_0 of the stationary observer $\Omega = 0$ and fixed $\theta_0 = \frac{\pi}{2}$, $a = 0.98$. The celestial sphere is at distance $r = 1000$.

-
- [1] Bardeen J M Timelike and null geodesics in the Kerr metric Black Holes, 1973, ed B DeWitt and C DeWitt (New York: Gordon and Breach) p 215
 - [2] Bizyaev I. A., Mamaev I. S., Bifurcation diagram and a qualitative analysis of particle motion in a Kerr metric, *Physical Review D*, 2022, vol. 105, 063003, 28 pp.
 - [3] Bolsinov A. V., Borisov A. V., Mamaev I. S., Topology and stability of integrable systems, *Russian Mathematical Surveys*, 2010, vol. 65, no. 2, pp. 259–318.
 - [4] Boyer R. H., Lindquist R. W. Maximal analytic extension of the Kerr metric, *Journal of mathematical physics*, 1967, vol. 8, no. 2, pp. 265–281.
 - [5] Carter B. Global structure of the Kerr family of gravitational fields, *Physical Review*, 1968, vol. 174, no. 5, p. 1559.
 - [6] Dokuchaev V. I., Nazarova N. O. Silhouettes of invisible black holes, *Physics-Uspekhi*, 2020, vol. 63, no. 6, p. 583.
 - [7] Dokuchaev V. I., Nazarova N. O. Gravitational lensing of a star by a rotating black hole, *JETP Letters*, 2017, vol. 106, pp. 637-642.
 - [8] Eisenhart L. P. Separable systems of Stäckel, *Ann. of Math.*, 1934, vol. 35, no. 2, pp. 284–305.
 - [9] Grenzebach A., Perlick V., Lämmerzahl C. Photon regions and shadows of Kerr-Newman-NUT black holes with a cosmological constant, *Physical Review D*, 2014, vol. 89, no. 12, p. 124004.
 - [10] Gralla S. E., Lupsasca A. Null geodesics of the Kerr exterior, *Physical Review D*, 2020, vol. 101, no. 4, p. 044032.
 - [11] Gralla S. E., Lupsasca A. Lensing by Kerr black holes, *Physical Review D*, 2020, vol. 101, no. 4, p. 044031.
 - [12] James O. Tunzelmann E., Franklin P., Thorne K. S. Gravitational lensing by spinning black holes in astrophysics, and in the movie *Interstellar*, *Classical and Quantum Gravity*, 2015, vol. 32, no. 6, p. 065001.
 - [13] Felice F., Preti G. On the meaning of the separation constant in the Kerr metric, *Classical and Quantum Gravity*, 1999, vol. 16, no. 9, p. 2929.
 - [14] Luminet J. P. Image of a spherical black hole with thin accretion disk, *Astronomy and Astrophysics*, 1979, vol. 75, no. 1-2, p. 228-235.
 - [15] Müller T. GeoViS—Relativistic ray tracing in four-dimensional spacetimes, *Computer Physics Communications*, 2014, vol. 185, no. 8, pp. 2301-2308.
 - [16] Perlick V., Tsupko O. Y. Calculating black hole shadows: Review of analytical studies, *Physics Reports*, 2022, vol. 947, p. 1-39.
 - [17] Perlick V. Gravitational lensing from a spacetime perspective, *Living reviews in relativity*, 2004, vol. 7, pp. 1-117.
 - [18] Teo E. Spherical orbits around a Kerr black hole, *General Relativity and Gravitation*, 2021, vol. 53, 10.
 - [19] Semerák O. Stationary frames in the Kerr field, *General relativity and gravitation*, 1993, vol. 25, pp. 1041-1077.
 - [20] Velásquez-Cadavid J. M., Arrieta-Villamizar J. A., Lora-Clavijo F. D., Pimentel O. M., Osorio-Vargas J. E. OSIRIS: a new code for ray tracing around compact objects, *The European Physical Journal C*, 2022, vol. 82, no. 2, p. 103.